

Optical Excitations of Chlorophyll *a* and *b* Monomers and Dimers

María Rosa Preciado-Rivas,¹ Duncan John Mowbray,^{1,2,3, a)} Keenan Lyon,² Ask Hjorth Larsen,³ and Bruce Forbes Milne^{4,3,5}

¹⁾*School of Physical Sciences and Nanotechnology, Yachay Tech University, Urcuquí 100119, Ecuador*

²⁾*Department of Applied Mathematics, University of Waterloo, Canada N2L 3G1*

³⁾*Nano-Bio Spectroscopy Group and ETSF Scientific Development Centre, Departamento de Física de Materiales, Universidad del País Vasco UPV/EHU, E-20018 San Sebastián, Spain*

⁴⁾*CFisUC, Department of Physics, University of Coimbra, Rua Larga, 3004-516 Coimbra, Portugal*

⁵⁾*Coimbra Chemistry Center, Department of Chemistry, University of Coimbra, Rua Larga, 3004-535 Coimbra, Portugal*

A necessary first step in the development of technologies such as artificial photosynthesis is understanding the photoexcitation process within the basic building blocks of naturally-occurring light harvesting complexes (LHCs). The most important of these building blocks in biological LHCs such as LHC II from green plants are the chlorophyll *a* (Chl *a*) and chlorophyll *b* (Chl *b*) chromophores dispersed throughout the protein matrix. However, efforts to describe such systems are still hampered by the lack of computationally efficient and accurate methods that are able to describe optical absorption in large biomolecules. In this work we employ a highly efficient linear combination of atomic orbitals (LCAOs) to represent the Kohn–Sham (KS) wave functions at the density functional theory (DFT) level and perform time dependent density functional theory (TDDFT) in either the reciprocal space and frequency domain (LCAO-TDDFT- $k-\omega$) or real space and time domain (LCAO-TDDFT- $r-t$) calculations of the optical absorption spectra of Chl *a* and *b* monomers and dimers. We find our LCAO-TDDFT- $k-\omega$ and LCAO-TDDFT- $r-t$ calculations reproduce results obtained with a plane wave (PW) representation of the KS wave functions (PW-TDDFT- $k-\omega$), but with a significant reduction in computational effort. Moreover, by applying the GLLB-SC derivative discontinuity correction Δ_x to the KS eigenenergies, with both LCAO-TDDFT- $k-\omega$ and LCAO-TDDFT- $r-t$ methods we are able to semi-quantitatively reproduce the experimentally measured photoinduced dissociation (PID) results. This work opens the path to first principles calculations of optical excitations in macromolecular systems.

I. INTRODUCTION

Chlorophyll *a* (Chl *a* or $C_{55}H_{72}MgN_4O_5$) and chlorophyll *b* (Chl *b* or $C_{55}H_{70}MgN_4O_6$)^{1,2} are the fundamental functional units of the light harvesting complex (LHC II)³ present in green plants. For this reason, understanding the photoexcitation process within Chl *a* and *b* is of great importance in the development of technologies such as those involved in the optimization of food crop production^{4,5} and conversion of solar radiation into a usable form of energy directly through methods such as conventional solar cells^{6,7} or via subsidiary technologies such as photosynthetically-driven (bio)reactor systems for hydrogen combustion^{8–11}. Moreover, such information is more generally applicable to the *in silico* design and optimization of dye-sensitized solar cells¹², organic photovoltaic cells¹³, photocatalytic systems¹⁴, optoelectronic devices¹⁵, and plasmonics¹⁶.

Although much progress has been recently made in both the experimental measurement of individual monomer and dimer Chl *a* and *b* spectra^{17–19}, and their theoretical description at the time-dependent density functional theory (TDDFT)²⁰ level^{21–24}, the lack of reasonably accurate yet highly efficient computational methods has hampered efforts to describe the optical absorption of large Chl-containing biomolecules. Initial attempts to investigate the optical absorption characteristics of biomacromolecules such as the LHC II using first-

principles electronic structure methods have helped to clarify several aspects of the functioning of these systems^{25,26}. However, these calculations neglected the protein matrix, and thus failed to fully explain the role played by the surrounding proteins in photosynthesis and why they are produced. Moreover, the computational resources required for a complete treatment of systems of this size lie considerably beyond what is generally available to most researchers.

On the one hand, methods based on the Kohn–Sham (KS) density of states²⁷, while being quite efficient, often underestimate energy gaps by more than half. This is because an independent-particle picture fails to describe electronic screening of the excited states²⁸. On the other hand, quasiparticle-based calculations of spectra from the Bethe–Salpeter equation (BSE)²⁹, while often achieving quantitative accuracy, are extremely heavy computationally³⁰. As a result, only recently have even the smallest dye-sensitized solar cells (DSSC) been described at the BSE level³¹. Moreover, such methods are intrinsically ill-suited to the description of isolated and/or non-periodic systems.

Although TDDFT^{20,32} real time^{33–36} and frequency domain^{37–41} calculations provide an attractive alternative, implementations based on real-space (RS) or plane-wave (PW) representations of the KS orbitals²⁷ are both computationally expensive, and exhibit a strong exchange and correlation (xc) functional dependence for their accuracy. Time propagation RS (RS-TDDFT- $r-t$) calculations require time steps much shorter than what is needed to resolve the features of the spectra in order to ensure the stability of the calculation²⁵. Such

^{a)}Electronic mail: duncan.mowbray@gmail.com

instabilities of RS calculations may be related to their freedom in representing the KS wavefunctions, which are only constrained by the grid spacing.

In this work we employ linear combinations of atomic orbitals (LCAOs) to provide a more efficient representation of the KS orbitals, while retaining the accuracy of PW-based TDDFT reciprocal space and frequency domain PW-TDDFT- $k-\omega$ calculations of the optical absorption. Moreover, we use the recently developed derivative discontinuity correction based on the exchange part of the GLLB-SC⁴² functional Δ_x to correct the KS eigenenergies and provide a semi-quantitative agreement with experimental measurements^{43–45}. Furthermore, the constraints imposed by an LCAO representation of the KS wavefunctions may be expected to improve the stability of time-propagation TDDFT calculations (LCAO-TDDFT- $r-t$), allowing one to use larger time steps. However, the reliability of LCAO-TDDFT is inherently basis set dependent⁴⁶. This makes an assessment and benchmarking for the fundamental functional units with PW-TDDFT- $k-\omega$ calculations and photoinduced dissociation (PID) experiments essential before applying LCAO-TDDFT- $k-\omega$ or LCAO-TDDFT- $r-t$ to the complete macromolecular system.

By applying LCAO-TDDFT methods^{44,45,47,48} to the Chl *a* and *b* monomer and dimer systems, we may clearly explain their advantages and disadvantages for describing light-harvesting systems, with the aim of applying these methods to macromolecules such as the complete LHC II. Note that since experimental measurements of the Chl *b* dimer are currently unavailable, we have restricted consideration to the Chl *a* dimer herein.

This paper is organized as follows. In Sec. II we describe the computational parameters employed to model the Chl *a* and *b* systems and provide a theoretical background to LCAO-TDDFT- $k-\omega$ ^{44,45,47} and LCAO-TDDFT- $r-t$ ⁴⁸ calculations in the projector augmented wave (PAW) method. In Sec. III, we perform a basis set convergence test and direct comparison with PW-TDDFT- $k-\omega$ calculations and PID measurements for our LCAO-TDDFT- $k-\omega$ calculations of Chl *a* and *b*, model the excitonic density of their first four bright excitations ω_i using the electron hole density difference $\Delta\rho(\mathbf{r}, \omega_i)$ from LCAO-TDDFT- $k-\omega$, compare our LCAO-TDDFT- $r-t$ calculations with PID measurements for Chl *a* and *b*, compare both LCAO-TDDFT- $k-\omega$ and LCAO-TDDFT- $r-t$ calculations with PID measurements for the Chl *a* dimer (Chl *a*)₂, and finally tabulate and compare our results for the Q band with those available in the literature^{17,19}. We then provide concluding remarks in Sec. IV. Atomic units ($\hbar = e = m_e = a_0 = 1$) are employed throughout unless stated otherwise.

II. METHODOLOGY

All DFT^{27,49} calculations were performed using the PAW^{50–52} implementation within the GPAW code^{53–55}. We employed the generalized gradient approximation (PBE⁵⁶) for the exchange and correlation functional. To represent the electron density and wave functions we employed either LCAOs⁵⁵ with a double- ζ -polarized (DZP) basis set, after performing

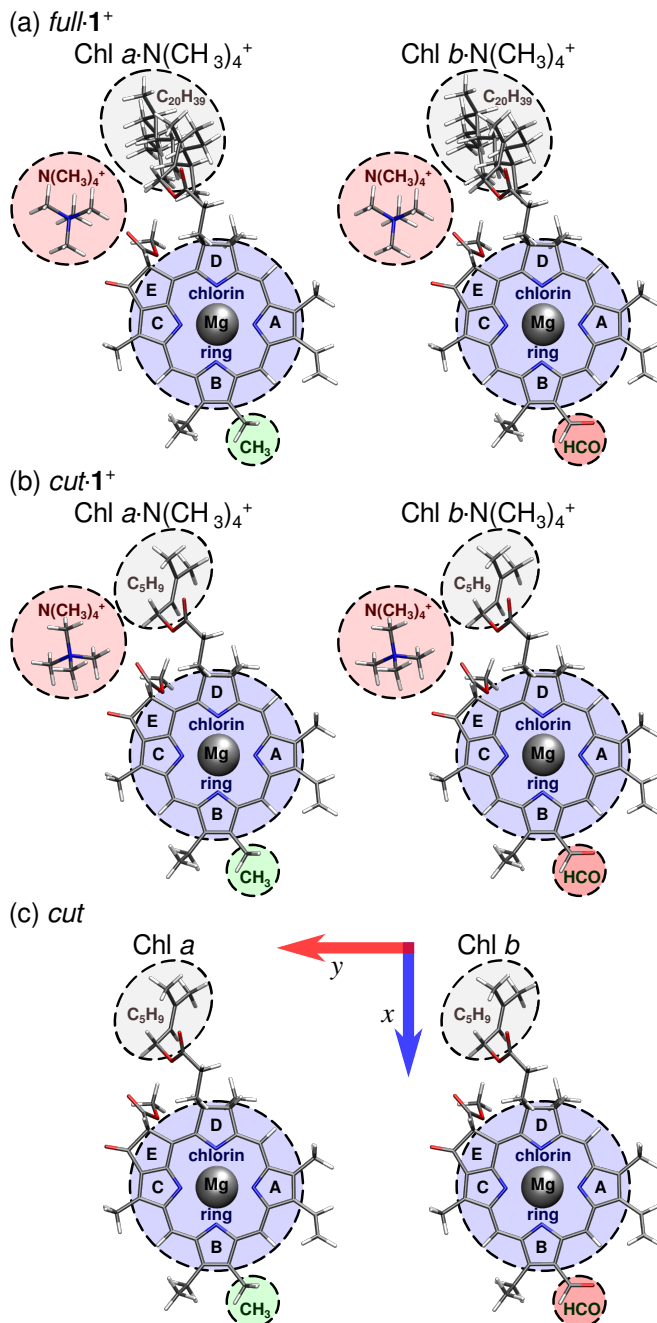


FIG. 1. Schematics of (a) *full-1*⁺, (b) *cut-1*⁺, and (c) *cut* chlorophyll *a* (Chl *a*) and chlorophyll *b* (Chl *b*) structures with Mg atom, chlorin ring (blue), methyl group (CH₃, green) or aldehyde (HCO, red) groups, full (C₂₀H₃₉, grey) or cut (C₅H₉, grey) hydrocarbon chain, and a tetramethylammonium charge tag (N(CH₃)₄⁺, red). Labelling of the rings (A–E) and orientation of the *x* and *y* polarization axes (blue and red arrows) is according to IUPAC-IUB nomenclature^{1,2}. Mg, C, O, N, and H atoms are depicted in silver, grey, red, blue, and white. Structures in (a) *full-1*⁺ are based on those provided in Ref. 17.

convergence tests with basis sets of varying quality up to a quadruple- ζ -polarized (QZP) basis set, or PWs with a plane-wave cutoff of 340 eV. Gas phase structures for the full Chl *a* and *b* monomers (see Figure 1(a) *full-1*⁺) and the Chl *a* dimer

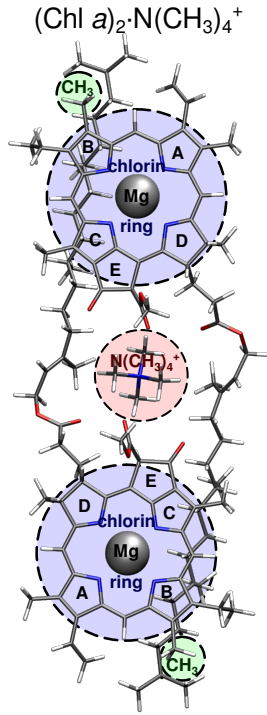


FIG. 2. Schematic of the chlorophyll *a* dimer (Chl *a*)₂ structure with Mg atom, chlorin ring (blue), methyl group (CH₃, green), and a tetramethylammonium charge tag (N(CH₃)₄⁺, red). Labelling of the rings (A–E) is according to IUPAC-IUB nomenclature^{1,2}. Mg, C, O, N, and H atoms are depicted in silver, grey, red, blue, and white. The structure is based on the linear configuration provided in Ref. 19.

(see Figure 2) were based on those of Refs. 17 and 19, respectively. To determine the influence of the hydrocarbon chain and the tetramethylammonium charge tag (N(CH₃)₄⁺ or **1**⁺) on the optical absorbance of Chl *a* and *b* monomers we have also considered structures with the hydrocarbon chain cut from C₂₀H₃₉ to C₅H₉ with and without the N(CH₃)₄⁺ charge tag, as shown in Figure 1 (a) *cut-1*⁺ and (b) *cut*, respectively.

Each structure was optimized using the ASE code^{57,58} until a maximum force less than 0.03 eV/Å was obtained. All structures were modelled in supercells with more than 6 Å of vacuum using non-periodic boundary conditions, that is, the electron density and wave functions were set to zero at the cell boundary. This prevents long-range interactions between repeated images that would affect a periodic calculation. More importantly, the use of non-periodic boundary conditions has been previously shown to be essential for modelling charged structures in gas phase⁵⁹.

Optical absorbance spectra were modelled using the imaginary part of the dielectric function, Im[$\epsilon(\omega)$], from LCAO-TDDFT calculations in the frequency domain (LCAO-TDDFT-*k*- ω)^{44,45,47,60}, and using the Fourier transform of the dipole moment, $\mathcal{F}\{d_m(t)\}$, from LCAO-TDDFT in the real time domain (LCAO-TDDFT-*r*-*t*)⁴⁸.

The optical absorbance from LCAO-TDDFT-*k*- ω in the $\hat{\mathbf{e}}_{\mathbf{q}}$

direction, neglecting local field effects, is given by^{44,45}

$$\text{Im}[\epsilon(\omega)] = \frac{1}{\Omega} \sum_{nm} \frac{4\pi\eta[f(\epsilon_m) - f(\epsilon_n)]}{(\omega - \epsilon_n + \epsilon_m - \Delta_x)^2 + \eta^2} \left| \frac{\hat{\mathbf{e}}_{\mathbf{q}} \cdot \langle \psi_n | \nabla | \psi_m \rangle}{\epsilon_n - \epsilon_m + \Delta_x} \right|^2 \quad (1)$$

where Ω is the supercell volume, η is the electronic broadening, f is the Fermi–Dirac function, ϵ_n is the eigenenergy and ψ_n is the KS wave function of the n th orbital, and Δ_x is the derivative discontinuity correction to the eigenenergies⁴² from the exchange part of the GLLB-SC functional given by⁴⁴

$$\Delta_x = \frac{8\sqrt{2}}{3\pi^2} \sum_{n=1}^N \left(\sqrt{\epsilon_{N+1} - \epsilon_n} - \sqrt{\epsilon_N - \epsilon_n} \right) \langle \psi_{N+1} | \frac{\psi_n^* \psi_n}{\rho} | \psi_{N+1} \rangle, \quad (2)$$

where N is the number of electrons. Incorporating this derivative discontinuity correction has been shown to provide better agreement with experimental band gaps⁴³ and optical absorption spectra^{44,45}.

The matrix elements in Eq. (1) may be expressed as⁴⁷

$$\langle \psi_n | \nabla | \psi_m \rangle = \sum_{\mu\nu} c_{\nu n}^* c_{\mu m} \langle \tilde{\phi}_\nu | \mathcal{T}^\dagger \nabla \mathcal{T} | \tilde{\phi}_\mu \rangle, \quad (3)$$

where the sum is over $\mu \equiv \{i, a\}$ for the i th state centered on atom a , $\tilde{\phi}_\mu$ are the localized basis functions, so that $|\tilde{\psi}_m\rangle = \sum_\mu c_{\mu m} |\tilde{\phi}_\mu\rangle$ with coefficients $c_{\mu m}$ for the m th KS wave function, and \mathcal{T} is the PAW transformation operator^{50–52}

$$\mathcal{T} = 1 + \sum_{ai} (|\varphi_i^a\rangle - |\tilde{\varphi}_i^a\rangle) \langle \tilde{p}_i^a|, \quad (4)$$

where $\tilde{\varphi}_i^a$ and φ_i^a are the pseudo and all-electron partial waves for state i on atom a within the PAW formalism, and $|\tilde{p}_i^a\rangle$ are the smooth PAW projector functions.

Since the matrix elements of Eq. (3) must already be calculated to obtain the forces at the DFT level, the calculation of Im[$\epsilon(\omega)$] using Eq. (1) simply involves the multiplication of previously calculated matrices. For this reason, the calculation of Im[$\epsilon(\omega)$] using LCAO-TDDFT-*k*- ω is very efficient, with scaling of $O(NM^2)$ or better⁶¹, where N is the number of KS wavefunctions and $M \geq N$ is the total number of basis functions used in the LCAO calculation. This provides a significant speed-up compared to the $O(N^5)$ scaling of the Casida LCAO-TDDFT-*r*- ω formalism^{37,38,48}. We found ten unoccupied KS wave functions per chlorophyll molecule were already sufficient to converge the spectra up to 3.5 eV. This is because local field effects may be safely neglected in the optical limit for gas phase structures^{41,47}.

The optical absorbance from LCAO-TDDFT-*r*-*t* is given by the Fourier transform of the dipole moment, d_m , so that

$$\mathcal{F}\{d_m(t)\} = \frac{1}{\pi\mathcal{K}} \int \sin(\omega t) e^{-\frac{t^2}{2\sigma^2}} [d_m(t) - d_m(0)] dt \quad (5)$$

where $\mathcal{K} = 1 \times 10^{-5}$ is the strength of the “kick” in the $\hat{\mathbf{e}}_{\mathbf{q}}$ direction, and σ is the peak broadening. The dipole moment is then obtained from the time dependent charge density $\rho(\mathbf{r}, t)$ using

$$d_m(t) = - \iiint \rho(\mathbf{r}, t) (\mathbf{r} \cdot \hat{\mathbf{e}}_{\mathbf{q}}) dV. \quad (6)$$

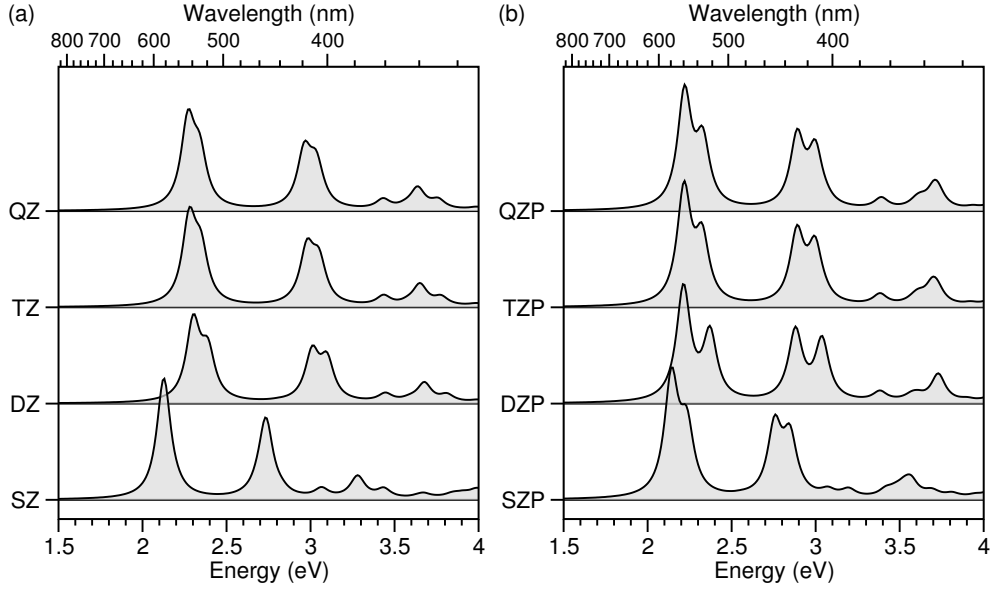


FIG. 3. Dependence of the LCAO-TDDFT- k - ω optical absorption spectra of Chl *a* on the single- ζ (SZ), double- ζ (DZ), triple- ζ (TZ) and quadruple- ζ (QZ) LCAO basis sets (a) without and (b) with polarization (P) functions.

The time dependent charge density is simply $\rho(\mathbf{r}, t) = -e \sum_n f(\varepsilon_n) |\psi_n(\mathbf{r}, t)|^2$, where $\psi_n(\mathbf{r}, t)$ are the time-dependent KS wave functions which are obtained by propagating

$$i \frac{\partial}{\partial t} \psi_n(\mathbf{r}, t) = \mathcal{H}_{\text{KS}}(t) \psi_n(\mathbf{r}, t), \quad (7)$$

where $\mathcal{H}_{\text{KS}}(t) = -\frac{1}{2} \nabla^2 + v_{\text{KS}}[\rho(\mathbf{r}, t)](\mathbf{r}, t)$ is the KS Hamiltonian for independent electrons, and v_{KS} is the KS potential functional.

Employing LCAO to represent the time-dependent KS wave functions, we may express Eq. (7) as⁴⁸

$$\sum_{\mu} i \langle \tilde{\phi}_{\nu} | \mathcal{T}^{\dagger} \mathcal{T} | \tilde{\phi}_{\mu} \rangle \frac{\partial}{\partial t} c_{\mu\nu}(t) = \sum_{\mu, m} \langle \tilde{\phi}_{\nu} | \mathcal{T}^{\dagger} \mathcal{H}_{\text{KS}}^{mm}(t) \mathcal{T} | \tilde{\phi}_{\mu} \rangle c_{\mu m}(t). \quad (8)$$

After applying the initial kick, the time propagation is performed using the reliable and numerically stable semi-implicit Crank–Nicolson method⁶², as described in Ref. 48.

As was the case for LCAO-TDDFT- k - ω , each step of the LCAO-TDDFT- r - t is very efficient and involves solving the system of linear equations, Eq. (8), with ScaLAPACK⁶¹. For this reason, the calculation of $\mathcal{F}\{d_m(t)\}$ using LCAO-TDDFT- r - t scales as $O(NM^2)$. Although this is worse than the $O(NG)$ scaling of RS-TDDFT- r - t , where G is the number of grid points, the constant prefactor for the grid propagation is so large that even for systems with thousands of electrons it is outperformed by several orders of magnitude by LCAO-TDDFT- r - t ⁴⁸.

All spectra have been calculated with intrinsic widths of 50 meV. In the frequency domain we employed an electronic broadening of $\eta = 50$ meV to the individual Lorentzian peaks, while in the real time domain we convoluted the dipole moment with a Gaussian of width $\sigma \approx 13$ fs.

The LCAO-TDDFT- r - t spectra remained stable with a 0.01 fs time step, which was sufficient to resolve the shape

of the dipole spectra. Such a time step is an order of magnitude greater than the 0.002 fs time step required for real space time propagation calculations to maintain stability²⁵. We were thus easily able to propagate up to 80 fs, twice that recorded with real space methods²⁵.

To provide insight into the spatial distribution of the exciton, we employ the electron hole density difference, $\Delta\rho(\mathbf{r}, \omega) = \rho_h(\mathbf{r}, \omega) + \rho_e(\mathbf{r}, \omega)$, as described in Refs. 31,44,45. Here, the electron/hole densities $\rho_{e/h}(\mathbf{r})$ are obtained by averaging the two-particle exciton density $\rho_{ex}(\mathbf{r}_e, \mathbf{r}_h)$, with respect to the hole/electron coordinate $\mathbf{r}_{h/e}$. We calculate the electron hole density difference $\Delta\rho(\mathbf{r}, \omega)$ for the first four bright excitations using the transitions from LCAO-TDDFT- k - ω . Since these molecular transitions are both well separated and composed of single transitions $m \rightarrow n$ at the LCAO-TDDFT- k - ω level, we find $\Delta\rho(\mathbf{r}, \omega_{mn}) \approx e(|\psi_n|^2 - |\psi_m|^2)$, where ψ_m and ψ_n are the KS orbitals corresponding to the hole and electron, respectively, and $\omega_{mn} \approx \varepsilon_n - \varepsilon_m + \Delta_x$ is the energy of the transition $m \rightarrow n$, including the derivative discontinuity correction Δ_x of Eq. (2).

III. RESULTS AND DISCUSSION

In Figure 3 we show the optical absorption spectrum of the neutral *cut* structure of Chl *a* calculated using either multiple- ζ basis sets (SZ, DZ, TZ and QZ) or the polarized versions of the basis sets (SZP, DZP, TZP and QZP) within the LCAO mode of the GPAW code. We systematically increase the number of functions to assess the sensitivity of the optical absorbance and observe that the spectrum converges differently for basis sets with and without polarization functions.

It can be seen in Figure 3(a) that the SZ basis set yields a red-shifted spectrum compared to the other spectra, the TZ

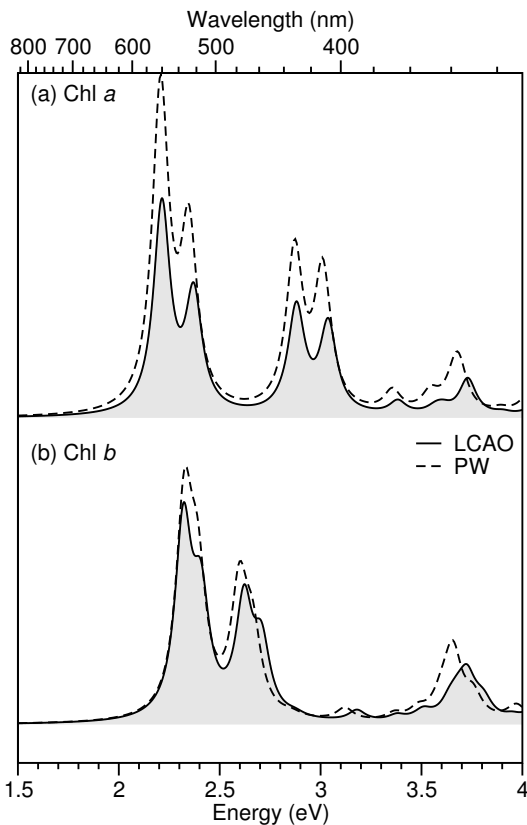


FIG. 4. Optical absorption of Chl *a* and *b* employing LCAO (solid lines, LCAO-TDDFT- k - ω) and PW (dashed lines, PW-TDDFT- k - ω) representations of the Kohn-Sham orbitals.

and QZ basis sets spectra are almost the same, and the DZ basis set yields the same energies of the Q and Soret bands compared to those of the TZ and QZ but the peaks within the band are more separated than in the TZ or QZ spectra. The polarized multiple- ζ basis sets are shown in Figure 3(b) and we observe that the SZP basis set also yields a red-shifted spectra compared to other spectra and there are more peaks above 3 eV. The spectra obtained using TZP and QZP are nearly identical and the DZP basis set yields the same energy of the Q and the Soret bands although the peaks within the bands are a little bit separated when compared to TZP and QZP.

Even though it seems that the spectrum of Chl *a* will not change if we increase the number of functions of the basis set, we cannot rely solely on these results to claim that an LCAO basis set will guarantee an accurate description of the optical absorption spectra. This is because LCAO basis sets cannot be systematically converged to the complete basis set limit, for molecules of this size. This is clear from comparing the result of the inclusion of polarization functions with the LCAO basis sets in Figure 3. Although double- ζ basis sets are converged with respect to the number of radial functions, the inclusion of polarization systematically alters the spectra. For this reason, we must compare the spectra of Chl *a* and Chl *b* obtained using LCAO and a PW representations of the KS wavefunctions.

In Figure 4, we show the optical absorption spectra of the

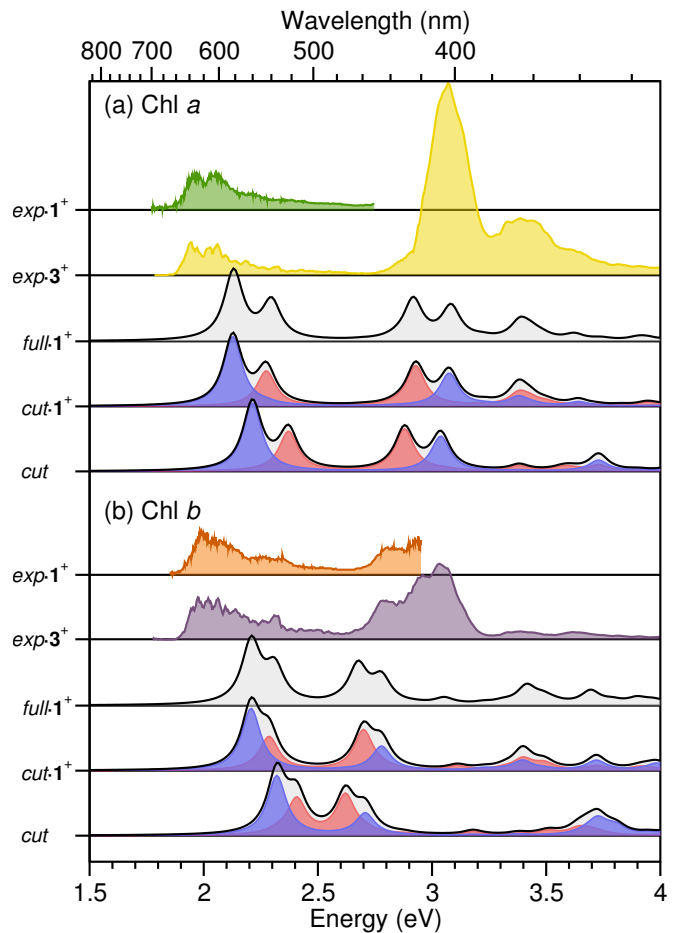


FIG. 5. Optical absorbance spectra, $\text{Im}[\epsilon(\omega)]$, from LCAO-TDDFT- k - ω for (a) Chl *a* and (b) Chl *b* *full-1+*, *cut-1+*, and *cut* structures, with spectra decomposed into absorption in the *x* (blue) or *y* (red) polarization directions^{1,2}, as shown in Figure 1. These are compared with those measured experimentally with tetramethylammonium and acetylcholine charge tags, *exp-1+* and *exp-3+*, respectively, from Refs. 17 and 18.

cut structures of both Chl *a* and Chl *b* calculated using either the DZP basis set within the LCAO mode, or using a PW representation of the KS wavefunctions that ensures converged optical absorption spectra. We find that the DZP basis set yields an optical absorption spectrum with transition energies very close to those of the spectrum calculated using PW. We observe that the LCAO spectra is only slightly (much smaller than the 0.1 eV DFT accuracy) red-shifted compared to the PW spectra, but underestimates the intensities of the transitions. Nevertheless, we can affirm that the atomic basis set with double- ζ and polarization functions, DZP, is sufficient to ensure semi-quantitative agreement of the optical absorption spectra for the Chl *a* and Chl *b* with the PW calculations.

The DZP basis sets have been shown to be sufficient (and often necessary) to converge to the results calculated with PW representations of the KS wavefunctions in other works as well^{55,63}. From hereon we shall restrict consideration to the DZP basis set and simply refer to our calculations as LCAO.

In Figure 5 we plot the spectra obtained from LCAO-

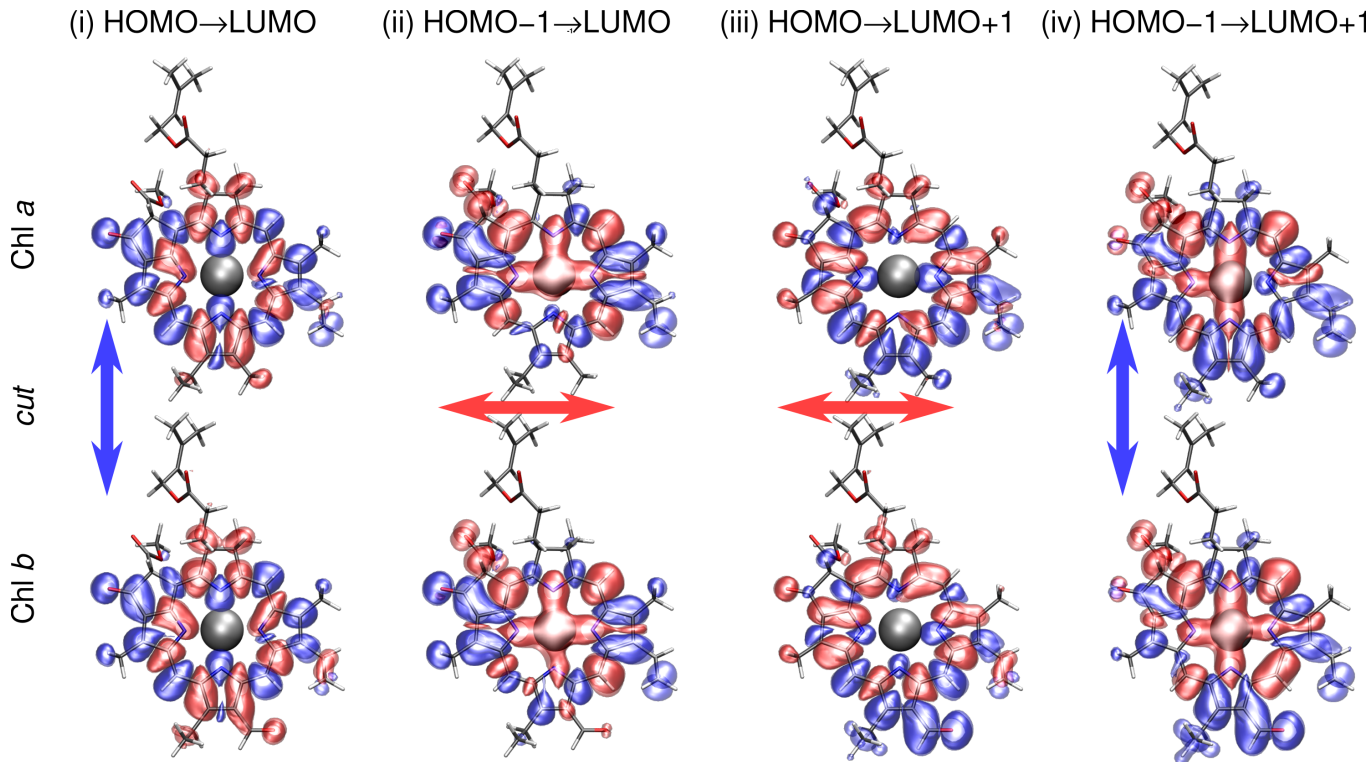


FIG. 6. Isosurfaces of the electron (blue) and hole (red) density difference $\Delta\rho(\mathbf{r}, \omega_i) = \pm 0.001 e/\text{\AA}^3$ of the first four excitations at ω_i of neutral Chl *a* and *b* with a cut hydrocarbon chain (*cut*) (i) HOMO \rightarrow LUMO, (ii) HOMO-1 \rightarrow LUMO, (iii) HOMO \rightarrow LUMO+1, and (iv) HOMO-1 \rightarrow LUMO+1. Absorption is along the N-Mg-N bonds either in the *x* (blue arrows) or *y* (red arrows) polarization directions^{1,2}. Mg, C, O, N, and H atoms are depicted in silver, grey, red, blue, and white.

TDDFT- k - ω including the derivative discontinuity correction Δ_x for the Chl *a* and *b* monomers shown in Figure 1. The onset of the calculated spectra are in semi-quantitative agreement with the experimental spectra obtained with either the monocationic tetramethylammonium 1^+ or acetylcholine 3^+ tag. The difference between the maximum of the Q band and the calculated first excitation energy is less than 0.2 eV and the difference between the maximum of the Soret band and the calculated fourth excitation is less than 0.1 eV. Also, the spectra of the *cut*- 1^+ structure shows the same qualitative behavior as the *full*- 1^+ structure, suggesting that none to negligible changes in the optical absorption spectra are caused by the carbon chain. However, when the charge tag is removed, that is, regarding the *cut* structure, the Q band peaks are blue shifted and the band gap is widened, whereas the Soret band peaks are red shifted.

For Chl *b*, Figure 5(b), the calculated spectra for the *full*- 1^+ structure is also in semi-quantitative agreement with the experimental spectra. Specifically, the peaks of the Q band and the Soret band of the *full*- 1^+ structure are blue and red shifted, respectively, when compared to the experimental data, with a difference between the Q band maximum and the calculated first excitation of 0.23 eV and a difference between the Soret band maximum and the calculated fourth excitation of 0.26 eV. Again, the spectrum of the *cut*- 1^+ structure is qualitatively the same as the spectrum of the *full*- 1^+ , reinforcing the idea that the carbon chain has no impact in the optical absorbance

and that it should be centered on the Mg atom and the chlorin ring. When removing the charge tag (*cut* structure) the Q band peaks are again blue shifted, and the band gap is widened, whereas the Soret band peaks are red shifted.

The intensities of the excitations of the Soret band are being underestimated about 75% for Chl *a* and 52% for Chl *b*, comparing the *full*- 1^+ to the experimental data. Also, the intensity of the Soret band peaks is less compared to that of the Q band peaks. This is not the case for the experimental data. Although the relative intensities are adjusted, that is, the Soret band peaks intensities are increased by applying the GLLB-SC correction to the spectra following Eq. 1, they are still underestimated.

Such a difference can be explained by the fact that we are neglecting charge transfer excitations at the linear density response level. The higher intensity of these peaks is often attributed in the literature to this type of charge transfer excitation¹⁷, which we are unable to model at the LCAO-TDDFT- k - ω level. In this way, our underestimation of the Soret band intensity provides indirect insight into the nature of the experimentally observed peaks.

In Figure 6 we plot the spatial distribution of the electron and hole densities for the first four bright transitions of the Chl *a* and *b* *cut* structures. As shown in Figure 5, the first and fourth excitations are induced by optical absorption along the N-Mg-N bond in the *x* polarization direction^{1,2} (blue arrows in Figure 6), while the second and third excitations

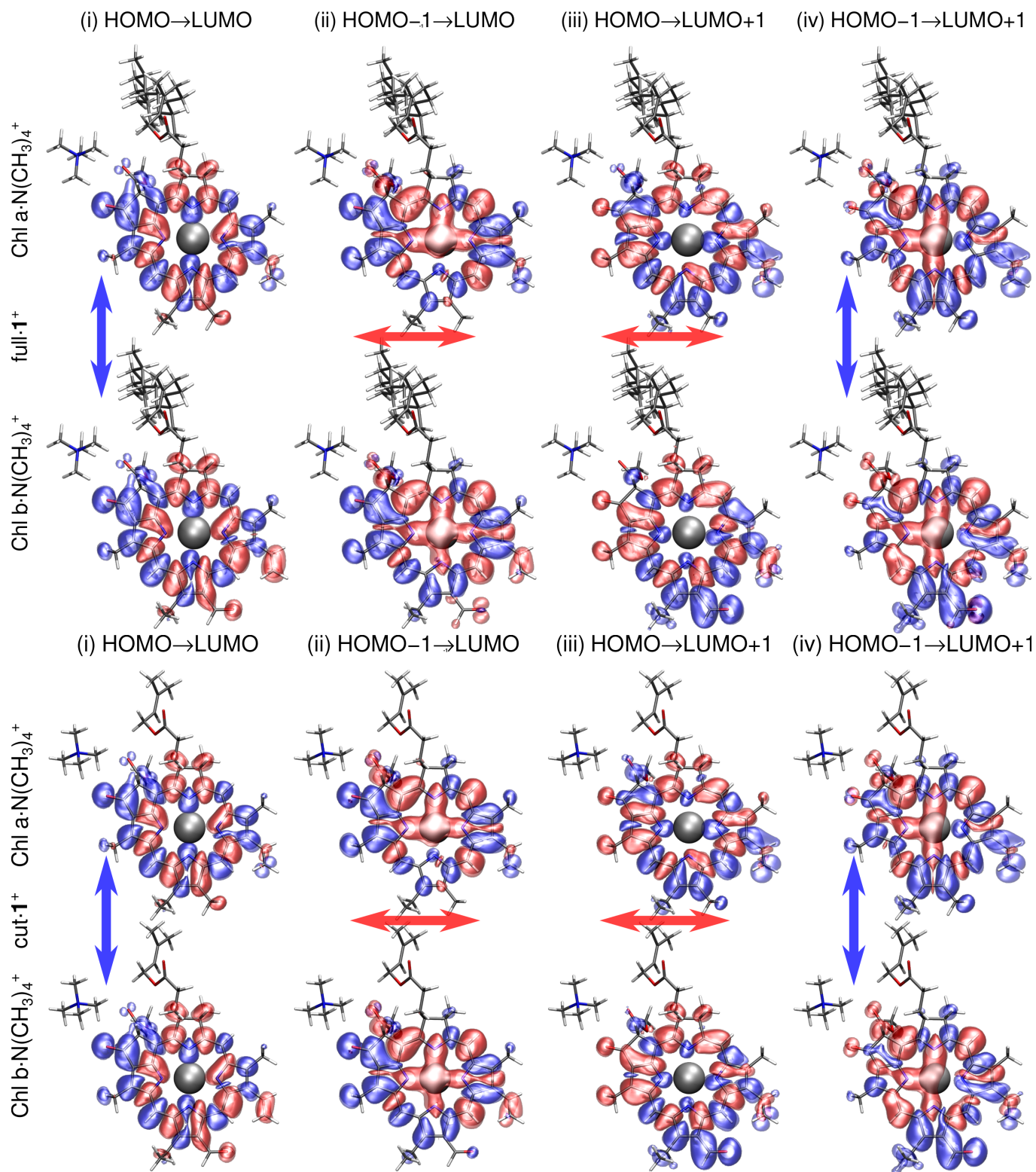


FIG. 7. Isosurfaces of the electron (blue) and hole (red) density difference $\Delta\rho(\mathbf{r}, \omega_i) = \pm 0.001e/\text{\AA}^3$ of the first four excitations ω_i of charge-tagged Chl *a*-N(CH₃)₄⁺ and Chl *b*-N(CH₃)₄⁺ with a full (full-1⁺, upper panel) and cut (cut-1⁺, lower panel) hydrocarbon chain (i) HOMO → LUMO, (ii) HOMO-1 → LUMO, (iii) HOMO → LUMO+1, and (iv) HOMO-1 → LUMO+1. Mg, C, O, N, and H atoms are depicted in silver, grey, red, blue, and white.

are induced by optical absorption along the *y* polarization direction^{1,2} (red arrows in Figure 6), as expected. In each case,

the excitations are $\pi \rightarrow \pi$ transitions involving the two highest occupied molecular orbitals (HOMOs) and the two lowest unoccupied molecular orbitals (LUMOs).

For both species the electron density of the first and third excitations has weight on the $2p_z$ levels of the N atoms parallel to the direction of excitation towards the Mg atom. Conversely, the hole density of the second and third excitations on both Chl *a* and *b* has significant weight on the $2p_z$ levels of both the N and Mg atoms. Overall, the first and third transitions tend to move charge density from the chlorin ring to either its edges or towards the central Mg atom, whereas the second and fourth transitions tend to move charge from the central Mg atom to the edge of the chlorin ring along the direction of excitation.

Although the excitations for Chl *a* and *b* are qualitatively the same, we do notice differences in the region of the methyl/aldehyde. Specifically, the electron of the third and fourth transitions has significantly more weight around the aldehyde group of Chl *b* compared to the methyl group of Chl *a*. Also, the hole density of the second and fourth transitions has weight on all four N atoms for Chl *b*, whereas the electron density has some weight on one of the N atoms perpendicular to the direction of excitation.

Finally, the excitations of the charge tagged species with a cut (*cut* $\cdot 1^+$) and full (*full* $\cdot 1^+$) hydrocarbon chain, shown in Figure 7, are basically the same as those for the neutral species (*cut* shown in Figure 6). This provides additional evidence justifying the experimental use of charge tagged Chl *a* and *b* molecules to describe the optical absorption of the neutral isolated species^{17,18}.

In Figure 8 we directly compare the spectra obtained from LCAO-TDDFT-*r-t* for the Chl *a* and *b* monomers shown in Figure 1 with those measured experimentally from Refs. 17 and 18. The Q-band energy or onset of the LCAO-TDDFT-*r-t* spectra agrees quantitatively with that measured experimentally for both Chl *a* and *b* in Refs. 17 and 18. However, whereas we found distinct Q band transitions with polarizations in the *x* and *y* directions for LCAO-TDDFT-*k- ω* (see Figure 5), with LCAO-TDDFT-*r-t* we find the Q band transitions coincide in energy. Moreover, for Chl *b* *cut* $\cdot 1^+$, we find that whereas there are two Q-band peaks, they both have polarization in the *x* direction, from ring **B** to ring **D** along the N–Mg–N bond. This splitting of the Q band peak in the *x* direction and the weak Q band peak in the *y* direction are both suppressed once the charge tag is removed (see Figure 8(b) *cut*).

While we find removing the charge tag induces a blue shift of the Q band for Chl *a* and *b*, as was the case for LCAO-TDDFT-*k- ω* , we find the Soret band is less affected by the charge tag with LCAO-TDDFT-*r-t*. In the region of the Soret band LCAO-TDDFT-*r-t* yields many peaks from 2.5–4 eV. This may be related to the difficulty in converging higher energy peaks with TDDFT-*t*, although our time propagation of ~ 80 fs should be sufficient to converge these peaks.

Overall, we find the spectra from LCAO-TDDFT-*r-t* provide excellent agreement with the experimentally measured spectra with tetramethylammonium (*exp* $\cdot 1^+$) and acetylcholine (*exp* $\cdot 3^+$) charge tags. This provides further evidence

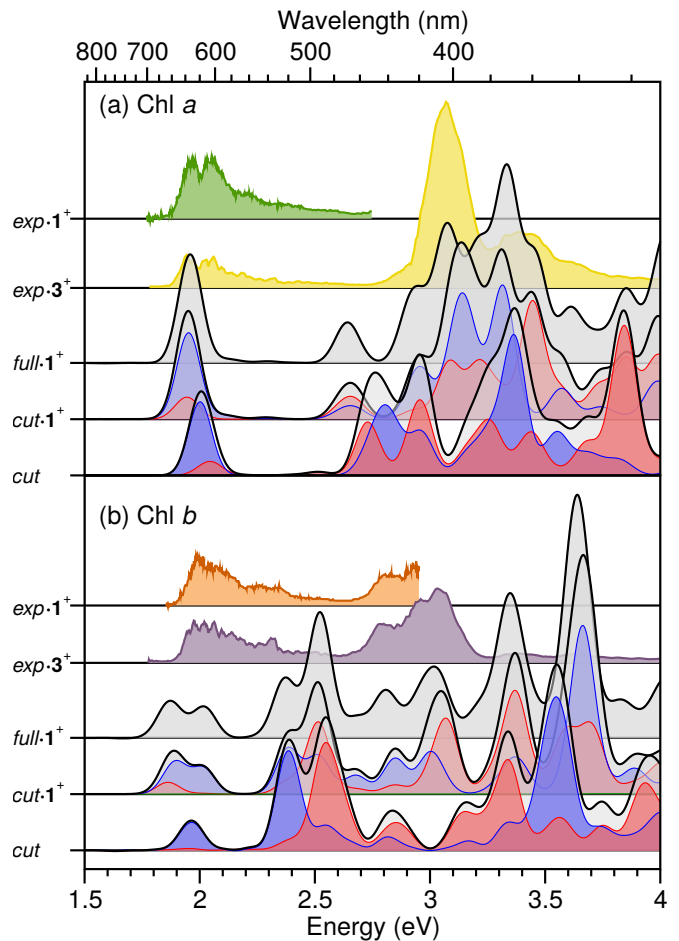


FIG. 8. Optical absorbance spectra, $\mathcal{F}\{d_m(t)\}$, from LCAO-TDDFT-*r-t* for (a) Chl *a* and (b) Chl *b* *full* $\cdot 1^+$, *cut* $\cdot 1^+$, and *cut* structures, with spectra decomposed into absorption in the *x* (blue) or *y* (red) polarization directions^{1,2}, as shown in Figure 1. These are compared with those measured experimentally with tetramethylammonium and acetylcholine charge tags, *exp* $\cdot 1^+$ and *exp* $\cdot 3^+$, respectively, from Refs. 17 and 18.

that the exact structure of the charge tag has little to no impact on the onset of the spectra^{17,18}. Moreover, the spectra exhibit rather minor changes upon removing the charge tag, providing further justification for using charge tagged Chl *a* and *b* to describe the optical absorption of the neutral isolated species^{17,18}.

Going beyond the monomer, in Figure 9 we directly compare the optical absorbance spectra for the Chl *a* dimer measured experimentally from Ref. 19, obtained from LCAO-TDDFT-*k- ω* , $\text{Im}[\epsilon(\omega)]$, and LCAO-TDDFT-*r-t*, $\mathcal{F}\{d_m(t)\}$. In both cases, the experimental onset of the peak is reproduced semi-quantitatively, with the derivative discontinuity corrected LCAO-TDDFT-*k- ω* results somewhat blue shifted by about 0.2 eV. However, as was the case for the monomer, the experimentally observed splitting of the Q band is clearly visible with LCAO-TDDFT-*k- ω* but absent from the LCAO-TDDFT-*r-t* Chl *a* spectrum.

Overall, these results show that increasing the system size,

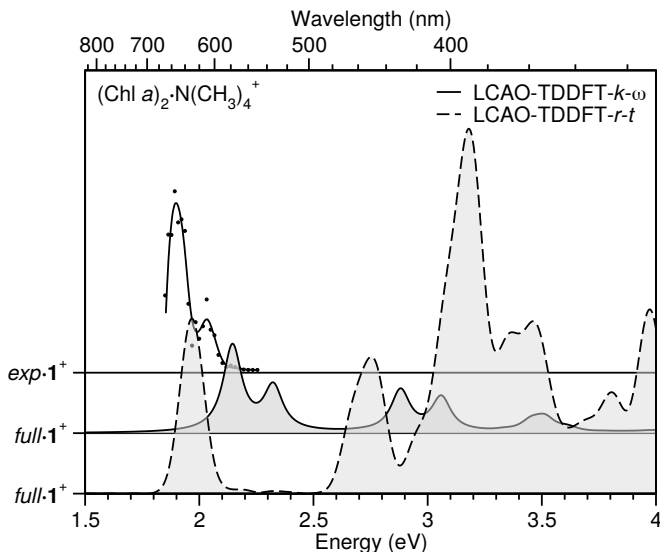


FIG. 9. Optical absorbance spectra from LCAO-TDDFT- $k-\omega$ (solid lines, $\text{Im}[\varepsilon(\omega)]$), and LCAO-TDDFT- $r-t$ (dashed lines, $\mathcal{F}\{d_m(t)\}$) for the $(\text{Chl } a)_2 \cdot \text{N}(\text{CH}_3)_4^+$ structure ($\text{full}\cdot\mathbf{1}^+$) shown in Figure 2 and as measured experimentally ($\text{exp}\cdot\mathbf{1}^+$, \bullet) from Ref. 19.

as we go from the monomer to the dimer, LCAO-TDDFT- $k-\omega$ and LCAO-TDDFT- $r-t$ provide the same level of accuracy. For LCAO-TDDFT- $k-\omega$, this means that after applying the derivative discontinuity correction $\Delta_x \approx 0.5$ eV, the spectra agree semi-quantitatively with the measured spectra for both the Chl a monomer and dimer. For LCAO-TDDFT- $r-t$, this correction is not required to obtain a quantitative description of the experimental spectra for both the Chl a monomer and dimer. Altogether, this suggests that for even larger systems, such as the LHC II, we may reasonably expect both LCAO-TDDFT- $k-\omega$ and LCAO-TDDFT- $r-t$ to continue to perform well.

In Table I we provide a direct comparison of the Q-band energy (first and second transitions shown in Figures 6 and 7) for Chl a , Chl b , and $(\text{Chl } a)_2$ obtained from PID measurements, TD-CAM-B3LYP/Def2-SVP calculations of the Casida LCAO-TDDFT- $r-\omega$ type^{37,38} using the imaginary part of the dynamic polarizability $\alpha(\omega)$ ($\frac{4\pi\omega}{c} \text{Im}[\alpha(\omega)]$), LCAO-TDDFT- $r-t$ ($\mathcal{F}\{d_m(t)\}$), PW-TDDFT- $k-\omega$ and LCAO-TDDFT- $k-\omega$ ($\text{Im}[\varepsilon(\omega)]$). Overall, we find excellent agreement between PID, LCAO-TDDFT- $r-t$, and TD-CAM-B3LYP/Def2-SVP. In fact, our LCAO-TDDFT- $r-t$ calculations perform somewhat better than TD-CAM-B3LYP/Def2-SVP for describing the Q band energies of Chl a , Chl b , and $(\text{Chl } a)_2$. These LCAO-TDDFT results, along with its computational speed-up, provide strong motivation for the future use of both LCAO-TDDFT- $k-\omega$ and LCAO-TDDFT- $r-t$ for describing larger systems such as the LHC II.

IV. CONCLUSIONS

We have shown that LCAO-TDDFT- $k-\omega$ ^{44,45,47} and LCAO-TDDFT- $r-t$ ⁴⁸ calculations are both significantly faster than

TABLE I. Q band energies in eV and wavelengths in nm for Chl a and b monomers and dimers with and without the $\mathbf{1}^+$ charge tag.

method	structure	Chl a		Chl b	
		(eV)	(nm)	(eV)	(nm)
PID ^a	$\text{exp}\cdot\mathbf{1}^+$	1.97	629	1.99	623
	$\text{full}\cdot\mathbf{1}^+$	2.08	596	2.15	577
$\frac{4\pi\omega}{c} \text{Im}[\alpha(\omega)]^b$	full	2.04	608	2.13	582
	$\text{full}\cdot\mathbf{1}^+$	1.96	633	1.87, 2.02	662, 615
$\mathcal{F}\{d_m(t)\}^c$	$\text{cut}\cdot\mathbf{1}^+$	1.95	636	1.89, 2.00	657, 621
	cut	2.01	618	1.96	631
$\text{Im}[\varepsilon(\omega)]^d$	$\text{full}\cdot\mathbf{1}^+$	2.13, 2.30	582, 540	2.21, 2.31	562, 537
	$\text{cut}\cdot\mathbf{1}^+$	2.13, 2.27	583, 545	2.21, 2.29	562, 542
$\text{Im}[\varepsilon(\omega)]^e$	cut	2.21, 2.37	561, 524	2.32, 2.41	534, 515
	cut	2.21, 2.35	561, 528	2.33, 2.39	533, 518
(Chl a) ₂					
PID ^f	$\text{exp}\cdot\mathbf{1}^+$	1.90	652		
	$\text{full}\cdot\mathbf{1}^+$	2.05	605		
$\mathcal{F}\{d_m(t)\}^c$	$\text{full}\cdot\mathbf{1}^+$	1.97	630		
	$\text{full}\cdot\mathbf{1}^+$	2.15, 2.32	578, 534		

^aPhotoinduced dissociation from Ref. 17. ^bTD-CAM-B3LYP/Def2-SVP from Ref. 17. ^cLCAO-TDDFT- $r-t$ from this work. ^dLCAO-TDDFT- $k-\omega$ from this work. ^ePW-TDDFT- $k-\omega$ from this work. ^fPhotoinduced dissociation from Ref. 19. ^gTD-CAM-B3LYP/Def2-SVP from Ref. 19.

their PW-TDDFT- $k-\omega$, TD-CAM-B3LYP/Def2-SVP, and RS-TDDFT- $r-t$ counterparts and also provide a similar level of accuracy to alternative TDDFT methods in the description of the optical absorption spectrum of the key photosynthetic light-harvesting molecules Chl a and b and the dimeric system $(\text{Chl } a)_2$. Specifically, our LCAO-TDDFT- $k-\omega$ and LCAO-TDDFT- $r-t$ calculations provide both a semi-quantitative and qualitative description of the spectra of chlorophyll monomers and dimers, with the former yielding a significant reduction in memory requirements compared to PW-TDDFT- $k-\omega$ and the latter yielding an order of magnitude speed-up compared to RS-TDDFT- $r-t$ calculations due to the increased numerical stability of LCAO-TDDFT- $r-t$. These results pave the way for future studies applying these highly efficient and accurate LCAO-TDDFT methods to the characterization of biomacromolecules, such as the LHC II, and the full understanding of the physical and chemical processes involved in photosynthesis.

ACKNOWLEDGMENTS

This work employed the Imbabura cluster of Yachay Tech University, which was purchased under contract No. 2017-024 (SIE-UIEY-007-2017), and the Quinde I super-computer of Public Company Yachay E. P., which was implemented under contract No. 0051-2015, corresponding to Component No. 7 of Group No. 2, Re-YACHAY-018-2015. D.J.M. thanks the management and operation

team of the Quinde I Supercomputer for their help and assistance in this project. A.H.L. acknowledges funding from the European Union's Horizon 2020 research and innovation program under grant agreement no. 676580 with The Novel Materials Discovery (NOMAD) Laboratory, a European Center of Excellence; the European Research Council (ERC-2010-AdG-267374); Spanish grant (FIS2013-46159-C3-1-P); and Grupos Consolidados (IT578-13). The Coimbra Chemistry Centre is supported by FCT, through the Project PEst-OE/UI0313/2014 and POCI-01-0145-FEDER-007630. B.F.M. thanks the Portuguese Foundation for Science and Technology (projects CENTRO-01-0145-FEDER-000014 and POCI-01-0145-FEDER-032229) and the Donostia International Physics Centre for financial support.

- ¹G. P. Moss, "Nomenclature of tetrapyrroles," *Euro. J. Biochem.* **178**, 277–328 (1988).
- ²H. Scheer, in *Chlorophylls and Bacteriochlorophylls: Biochemistry, Biophysics, Functions and Applications*, Advances in Photosynthesis and Respiration, Vol. 25 (Springer, Dordrecht, The Netherlands, 2006) Chap. 1, pp. 1–26.
- ³D. Siefertmann-Harms, "Carotenoids in photosynthesis. I. location in photosynthetic membranes and light-harvesting function," *Biochim. Biophysica Acta - Rev. Bioenerg.* **811**, 325–355 (1985).
- ⁴S. P. Long, "We need winners in the race to increase photosynthesis in rice, whether from conventional breeding, biotechnology or both," *Plant Cell Environ.* **37**, 19–21 (2014).
- ⁵D. K. Ray, N. D. Mueller, P. C. West, and J. A. Foley, "Yield trends are insufficient to double global crop production by 2050," *PLOS One* **8**, e66428 (2013).
- ⁶A. V. Ruban, M. P. Johnson, and C. D. P. Duffy, "Natural light harvesting: Principles and environmental trends," *Energy Environ. Sci.* **4**, 1643–1650 (2011).
- ⁷G. R. Fleming, G. S. Schlau-Cohen, K. Amarnath, and J. Zaks, "Design principles of photosynthetic light-harvesting," *Faraday Discuss.* **155**, 27–41 (2012).
- ⁸S. I. Allakhverdiev, V. Thavasi, V. D. Kreslavski, S. K. Zharmukhamedov, V. V. Klimov, S. Ramakrishna, D. A. Los, M. Mimuro, H. Nishihara, and R. Carpentier, "Photosynthetic hydrogen production," *J. Photochem. Photobiol. C: Photochem. Rev.* **11**, 101–113 (2010).
- ⁹H. Krassen, A. Schwarze, B. Friedrich, K. Ataka, O. Lenz, and J. Heberle, "Photosynthetic hydrogen production by a hybrid complex of photosystem I and [NiFe]-hydrogenase," *ACS Nano* **3**, 4055–4061 (2009).
- ¹⁰S. Berardi, S. Drouet, L. Francas, C. Gimbert-Surinach, M. Guttentag, C. Richmond, T. Stoll, and A. Llobet, "Molecular artificial photosynthesis," *Chem. Soc. Rev.* **43**, 7501–7519 (2014).
- ¹¹S. Y. Searle and C. J. Malins, "Will energy crop yields meet expectations?" *Biomass Bioenergy* **65**, 3–12 (2014).
- ¹²J. Gong, K. Sumathy, Q. Qiao, and Z. Zhou, "Review on dye-sensitized solar cells (DSSCs): Advanced techniques and research trends," *Renew. Sust. Energ. Rev.* **68**, 234–246 (2017).
- ¹³N. Agnihotri, "Computational studies of charge transfer in organic solar photovoltaic cells: A review," *J. Photochem. Photobiol. C: Photochem. Rev.* **18**, 18–31 (2014).
- ¹⁴R. Ahmad, Z. Ahmad, A. U. Khan, N. R. Mastoi, M. Aslam, and J. Kim, "Photocatalytic systems as an advanced environmental remediation: Recent developments, limitations and new avenues for applications," *J. Environ. Chem. Eng.* **4**, 4143–4164 (2016).
- ¹⁵X. Li, *Optoelectronic Devices: Design, Modeling, and Simulation*, 1st ed. (Cambridge University Press, New York, NY, USA, 2009).
- ¹⁶C. D. Geddes, ed., *Reviews in Plasmonics 2016*, 1st ed., Reviews in Plasmonics, Vol. 2016 (Springer, 2016).
- ¹⁷B. F. Milne, Y. Toker, A. Rubio, and S. Brøndsted Nielsen, "Unraveling the intrinsic color of chlorophyll," *Angew. Chem., Int. Ed. Engl.* **54**, 2170–2173 (2015).
- ¹⁸M. H. Stockett, L. Musbat, C. Kjær, J. Houmøller, Y. Toker, A. Rubio, B. F. Milne, and S. Brøndsted Nielsen, "The Soret absorption band of isolated chlorophyll *a* and *b* tagged with quaternary ammonium ions," *Phys. Chem. Chem. Phys.* **17**, 25793–25798 (2015).
- ¹⁹B. F. Milne, C. Kjær, J. Houmøller, M. H. Stockett, Y. Toker, A. Rubio, and S. Brøndsted Nielsen, "On the exciton coupling between two chlorophyll pigments in the absence of a protein environment: Intrinsic effects revealed by theory and experiment," *Angew. Chem., Int. Ed. Engl.* **55**, 6248–6251 (2016).
- ²⁰E. Runge and E. K. U. Gross, "Density-functional theory for time-dependent systems," *Phys. Rev. Lett.* **52**, 997–1000 (1984).
- ²¹L. Hedayatifar, E. Irani, M. Mazarei, S. Rasti, Y. T. Azar, A. T. Rezakhani, A. Mashaghi, F. Shayeganfar, M. Anvari, T. Heydari, A. R. Tabar, N. Nafari, M. A. Vesaghi, R. Asgari, and M. R. Rahimi Tabar, "Optical absorption and electronic spectra of chlorophylls *a* and *b*," *RSC Adv.* **6**, 109778–109785 (2016).
- ²²J. Linnanto and J. Korppi-Tommola, "Quantum chemical simulation of excited states of chlorophylls, bacteriochlorophylls and their complexes," *Phys. Chem. Chem. Phys.* **8**, 663–687 (2006).
- ²³A. Dreuw and M. Head-Gordon, "Failure of time-dependent density functional theory for long-range charge-transfer excited states: The zincbacteriochlorin–bacteriochlorin and bacteriochlorophyll–spheroidene complexes," *J. Am. Chem. Soc.* **126**, 4007–4016 (2004).
- ²⁴A. B. J. Parusel and S. Grimme, "A theoretical study of the excited states of chlorophyll *a* and pheophytin *a*," *J. Phys. Chem. B* **104**, 5395–5398 (2000).
- ²⁵J. Jorner-Somoza, J. Alberdi-Rodriguez, B. F. Milne, X. Andrade, M. A. L. Marques, F. Nogueira, M. J. T. Oliveira, J. J. P. Stewart, and A. Rubio, "Insights into colour-tuning of chlorophyll optical response in green plants," *Phys. Chem. Chem. Phys.* **17**, 26599–26606 (2015).
- ²⁶C. König and J. Neugebauer, "First-principles calculation of electronic spectra of light-harvesting complex II," *Phys. Chem. Chem. Phys.* **13**, 10475–10490 (2011).
- ²⁷W. Kohn and L. J. Sham, "Self-consistent equations including exchange and correlation effects," *Phys. Rev.* **140**, A1133–A1138 (1965).
- ²⁸A. Migani, D. J. Mowbray, A. Iacomino, J. Zhao, H. Petek, and A. Rubio, "Level alignment of a prototypical photocatalytic system: Methanol on TiO₂(110)," *J. Am. Chem. Soc.* **135**, 11429–11432 (2013).
- ²⁹E. E. Salpeter and H. A. Bethe, "A relativistic equation for bound-state problems," *Phys. Rev.* **84**, 1232–1242 (1951).
- ³⁰G. Onida, L. Reining, and A. Rubio, "Electronic excitations: Density-functional versus many-body Green's-function approaches," *Rev. Mod. Phys.* **74**, 601–659 (2002).
- ³¹D. J. Mowbray and A. Migani, "Optical absorption spectra and excitons of dye-substrate interfaces: Catechol on TiO₂(110)," *J. Chem. Theor. Comput.* **12**, 2843–2852 (2016).
- ³²M. A. L. Marques, C. A. Ullrich, F. Nogueira, A. Rubio, K. Burke, and E. K. U. Gross, eds., *Time-Dependent Density Functional Theory* (Springer, Berlin, Heidelberg, 2006).
- ³³K. Yabana and G. F. Bertsch, "Time-dependent local-density approximation in real time," *Phys. Rev. B* **54**, 4484–4487 (1996).
- ³⁴K. Yabana and G. F. Bertsch, "Time-dependent local-density approximation in real time: Application to conjugated molecules," *Int. J. Quant. Chem.* **75**, 55–66 (1999).
- ³⁵S. Ghosh, A. Andersen, L. Gagliardi, C. J. Cramer, and N. Govind, "Modeling optical spectra of large organic systems using real-time propagation of semiempirical effective hamiltonians," *J. Chem. Theory Comput.* **13**, 4410–4420 (2017).
- ³⁶K. J. Koh, T. S. Nguyen-Beck, and J. Parkhill, "Accelerating realtime TDDFT with block-orthogonalized Manby–Miller embedding theory," *J. Chem. Theory Comput.* **13**, 4173–4178 (2017).
- ³⁷M. E. Casida, "Time-dependent density functional response theory for molecules," in *Recent Advances in Density Functional Methods, Part I*, edited by D. P. Chong (World Scientific, Singapore, 1995) pp. 155–192.
- ³⁸M. E. Casida, "Time-dependent density-functional theory for molecules and molecular solids," *J. Mol. Struct. (Theochem.)* **914**, 3–18 (2009).
- ³⁹J. Yan, K. S. Thygesen, and K. W. Jacobsen, "Nonlocal screening of plasmons in graphene by semiconducting and metallic substrates: First-principles calculations," *Phys. Rev. Lett.* **106**, 146803 (2011).
- ⁴⁰J. Yan, J. J. Mortensen, K. W. Jacobsen, and K. S. Thygesen, "Linear density response function in the projector augmented wave method: Applications to solids, surfaces, and interfaces," *Phys. Rev. B* **83**, 245122 (2011).

- ⁴¹D. J. Mowbray, “Theoretical electron energy loss spectroscopy of isolated graphene,” *Phys. Status Solidi B* **251**, 2509–2514 (2014).
- ⁴²M. Kuisma, J. Ojanen, J. Enkovaara, and T. T. Rantala, “Kohn-Sham potential with discontinuity for band gap materials,” *Phys. Rev. B* **82**, 115106 (2010).
- ⁴³I. E. Castelli, T. Olsen, S. Datta, D. D. Landis, S. Dahl, K. S. Thygesen, and K. W. Jacobsen, “Computational screening of perovskite metal oxides for optimal solar light capture,” *Energy Environ. Sci.* **5**, 5814–5819 (2012).
- ⁴⁴M. R. Preciado-Rivas, V. A. Torres-Sánchez, and D. J. Mowbray, “Optical absorption and energy loss spectroscopy of single-walled carbon nanotubes,” (2019), arXiv:1907.08036.
- ⁴⁵K. Lyon, M. R. Preciado-Rivas, V. Despoja, and D. J. Mowbray, “LCAO-TDDFT- k - ω : Spectroscopy in the optical limit,” (2019), unpublished.
- ⁴⁶T. P. Rossi, S. Lehtola, A. Sakko, M. J. Puska, and R. M. Nieminen, “Nanoplasmonics simulations at the basis set limit through completeness-optimized, local numerical basis sets,” *J. Chem. Phys.* **142**, 094114 (2015).
- ⁴⁷L. N. Glanzmann, D. J. Mowbray, D. G. F. del Valle, F. Scotognella, G. Lanzani, and A. Rubio, “Photoinduced absorption within single-walled carbon nanotube systems,” *J. Phys. Chem. C* **120**, 1926–1935 (2015).
- ⁴⁸M. Kuisma, A. Sakko, T. P. Rossi, A. H. Larsen, J. Enkovaara, L. Lehtovaara, and T. T. Rantala, “Localized surface plasmon resonance in silver nanoparticles: Atomistic first-principles time-dependent density-functional theory calculations,” *Phys. Rev. B* **91**, 115431 (2015).
- ⁴⁹P. Hohenberg and W. Kohn, “Inhomogeneous electron gas,” *Phys. Rev.* **136**, B864–B871 (1964).
- ⁵⁰P. E. Blöchl, “Projector augmented-wave method,” *Phys. Rev. B* **50**, 17953–17979 (1994).
- ⁵¹P. E. Blöchl, C. J. Först, and J. Schimpl, “Projector augmented wave method: *Ab Initio* molecular dynamics with full wave functions,” *Bull. Mater. Sci.* **26**, 33–41 (2003).
- ⁵²C. Rostgaard, *Exact Exchange in Density Functional Calculations: An Implementation in the Projector Augmented Wave Method*, Master’s thesis, Technical University of Denmark, Kongens Lyngby, Denmark (2006).
- ⁵³J. J. Mortensen, L. B. Hansen, and K. W. Jacobsen, “Real-space grid implementation of the projector augmented wave method,” *Phys. Rev. B* **71**, 035109 (2005).
- ⁵⁴J. Enkovaara, C. Rostgaard, J. J. Mortensen, J. Chen, M. Dułak, L. Ferrighi, J. Gavnholt, C. Glinsvad, V. Haikola, H. A. Hansen, H. H. Kristofersen, M. Kuisma, A. H. Larsen, L. Lehtovaara, M. Ljungberg, O. Lopez-Acevedo, P. G. Moses, J. Ojanen, T. Olsen, V. Petzold, N. A. Romero, J. Stausholm-Møller, M. Strange, G. A. Tritsaris, M. Vanin, M. Walter, B. Hammer, H. Häkkinen, G. K. H. Madsen, R. M. Nieminen, J. K. Nørskov, M. Puska, T. T. Rantala, J. Schiøtz, K. S. Thygesen, and K. W. Jacobsen, “Electronic structure calculations with GPAW: A real-space implementation of the projector augmented-wave method,” *J. Phys.: Condens. Matter* **22**, 253202 (2010).
- ⁵⁵A. H. Larsen, M. Vanin, J. J. Mortensen, K. S. Thygesen, and K. W. Jacobsen, “Localized atomic basis set in the projector augmented wave method,” *Phys. Rev. B* **80**, 195112 (2009).
- ⁵⁶J. P. Perdew, K. Burke, and M. Ernzerhof, “Generalized gradient approximation made simple,” *Phys. Rev. Lett.* **77**, 3865 (1996).
- ⁵⁷S. R. Bahn and K. W. Jacobsen, “An object-oriented scripting interface to a legacy electronic structure code,” *Comput. Sci. Eng.* **4**, 56–66 (2002).
- ⁵⁸A. H. Larsen, J. J. Mortensen, J. Blomqvist, I. E. Castelli, R. Christensen, M. Dułak, J. Friis, M. N. Groves, B. Hammer, C. Hargus, E. D. Hermes, P. C. Jennings, P. B. Jensen, J. Kermode, J. R. Kitchin, E. L. Kolsbjerg, J. Kubal, K. Kaasbjerg, S. Lysgaard, J. B. Maronsson, T. Maxson, T. Olsen, L. Pastewka, A. Peterson, C. Rostgaard, J. Schiøtz, O. Schütt, M. Strange, K. S. Thygesen, T. Vegge, L. Vilhelmsen, M. Walter, Z. Zeng, and K. W. Jacobsen, “The atomic simulation environment—a python library for working with atoms,” *J. Phys.: Condens. Matter* **29**, 273002 (2017).
- ⁵⁹D. J. Mowbray, A. Migani, G. Walther, D. M. Cardamone, and A. Rubio, “Gold and methane: A noble combination for delicate oxidation,” *J. Phys. Chem. Lett.* **4**, 3006–3012 (2013).
- ⁶⁰The LCAO-TDDFT- k - ω code is available free of charge from gitlab.com/lcao-tddft-k-omega/lcao-tddft-k-omega.
- ⁶¹L. S. Blackford, J. Choi, A. Cleary, E. D’Azevedo, J. Demmel, I. Dhillon, J. Dongarra, S. Hammarling, G. Henry, A. Petitet, K. Stanley, D. Walker, and R. C. Whaley, *ScaLAPACK Users’ Guide* (Society for Industrial and Applied Mathematics, Philadelphia, PA, 1997).
- ⁶²J. Crank and P. Nicolson, “A practical method for numerical evaluation of solutions of partial differential equations of the heat conduction type,” *Proc. Camb. Phil. Soc.* **43**, 50–67 (1947).
- ⁶³M. Strange, I. S. Kristensen, K. S. Thygesen, and K. W. Jacobsen, “Benchmark density functional theory calculations for nanoscale conductance,” *J. Chem. Phys.* **128**, 114714 (2008).